Available at www.sciencedirect.com

ScienceDirect

http://www.elsevier.com/locate/biombioe

Modelling of grate combustion in a medium scale biomass furnace for control purposes

Robert Bauer [a,*], Markus Gölles [b], Thomas Brunner [b,c], Nicolaos Dourdoumas [a], Ingwald Obernberger [b,c]

[a] Institute of Automation and Control, Graz University of Technology, Kopernikusgasse 24, 8010 Graz, Austria
[b] BIOENERGY 2020+ GmbH, Inffeldgasse 21b, 8010 Graz, Austria
[c] BIOS BIOENERGIESYSTEME GmbH, Inffeldgasse 21b, 8010 Graz, Austria

ARTICLE INFO

Article history:
Received 14 October 2008
Received in revised form
6 December 2009
Accepted 9 December 2009
Available online 6 January 2010

Keywords:
Fixed bed
Grate combustion
Biomass
Modelling
Process control
Co-current heat and mass transfer

ABSTRACT

A new mathematical model for the grate combustion of biomass has been derived from physical considerations. Various models for grate combustion can already be found in the literature. Usually their intention is to simulate the real situation in a furnace as precisely as possible. Hence they are very detailed, typically consisting of many partial differential equations. However, because of their complexity they are useless for control purposes. The new model is very simple, consisting of only two ordinary differential equations, which makes it particularly suitable as a basis for model based control strategies. To verify the model, experiments were performed at a pilot scale furnace with horizontally moving grate. The pilot plant is a downscaled version (180 kW_{th}) of a typical medium scale furnace in terms of geometry and instrumentation. Comparison of the measured and calculated values shows good agreement.

1. Introduction

Grate combustion is a common and well developed technology for burning biomass fuels and municipal solid waste. Present-day plants are well designed, combining high thermal efficiency with low emissions of gaseous pollutants (CO, NO_x etc.). Contrary to the technically mature design, the commonly used control strategies are obsolete compared to the possibilities of modern control theory.

State-of-the-art control methods for nonlinear systems (e.g. a biomass furnace) include differential geometric techniques as well as Lyapunov-based approaches [1–4]. An important prerequisite for these sophisticated methods is a simple mathematical model of the system consisting of as few as possible low-order ordinary differential equations. This implies that the simple model describes reality more approximatively than other models might do, but this does not matter since inaccuracies of the model as well as disturbances are compensated by the controller.

Numerous models for the combustion process have been developed and enhanced, e.g. [5–19]. Despite many simplifying assumptions, these models are still very detailed and therefore too complex to be used as a basis for model based control strategies. The most promising attempt to derive a simple model suitable for control design originates from Van Kessel [20]. He started with a very simple and quite intuitive

* *Corresponding author*. Tel.: +43 316 8737036; fax: +43 316 8737028.
E-mail address: robert.bauer@tugraz.at (R. Bauer).
0961-9534/$ – see front matter © 2009 Elsevier Ltd. All rights reserved.
doi:10.1016/j.biombioe.2009.12.005

model, but had to admit that "it was not possible to receive a good agreement between the experimental and theoretical response". Subsequently, he improved his model, but had to recognise that "a good physical fully accepted explanation is not available" for his extensions.

In this article a simple model for the grate combustion of biomass is derived from physical considerations on the basis of a pilot scale furnace of the research centre BIOENERGY 2020+ (depicted in Section 4). An intensive literature review (Section 2) was conducted as a basis for further model development. It showed that experts assume two completely different burning behaviours for grate combustion counter-current with ignition at the top of the bed and co-current with ignition at the bottom of the bed (see Fig. 1).

It is obvious that the dynamic behaviour is completely different for the counter-current and co-current case. Prior to modelling, it is therefore important to determine the present combustion situation at the pilot scale furnace investigated (see Section 5.1). Based on the insight gained into the basic combustion situation, a simple model for co-current combustion (ignition at the bottom of the bed) is derived (Section 3). The model is based on two mass balances for water and dry fuel, in which results of both literature search and experiments are considered.

Finally, the model was verified by appropriate experiments at a pilot scale furnace with horizontally moving grate at full and partial load (Section 5.2).

2. Extended literature review

It is widely believed that the combustion process starts with ignition on the upper surface of the fuel bed due to radiation from the flames and the furnace walls. The generated heat is transported against the air flow and causes drying and devolatilization of the moist fuel below. As a result of the different directions of heat and air, the reaction front is very narrow and moves slowly against the air flow (thus "counter-current", see Fig. 1(a)). The papers cited in Section 1 [5–19] are based on this assumption.

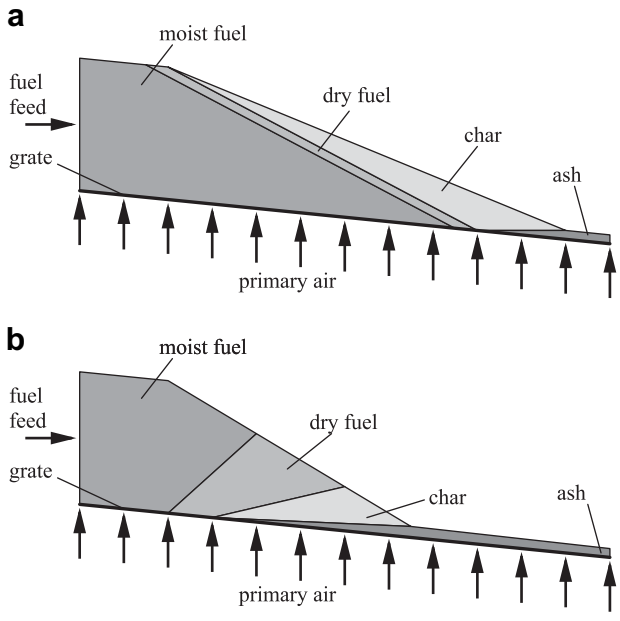

Fig. 1 – Different combustion behaviours: (a) counter-current with ignition at the top of the bed; (b) co-current with ignition at the bottom of the bed.

Only Thunman and Leckner [21,22] have suggested an ignition at the bottom of the bed, for example due to heat conduction through the grate bars. A thin layer of char is formed on the surface of the grate. The heat produced by the combustion of this char is transported both through the grate bars and with the gas flow. The hot gas dries and devolatilises new fuel above the char layer. This results in a broader reaction area moving in the same direction as the air (thus "co-current", see Fig. 1(b)). In [21], Thunman and Leckner described investigations at a reciprocating grate furnace (31 MW) as well as at pot furnaces (batch reactors). To sum up these investigations, some arguments indicating that co-current behaviour might be more common than previously thought are listed:

- Very moist fuel ($w = 50\%–60\%$) burns without any problem in the 31 MW furnace, but extinguishes at the same air flow in pot furnace experiments (which force counter-current behaviour).
- In the counter-current case, even the highest velocity of the reaction front would be too slow in comparison to the grate length of most furnaces (for the 31 MW furnace and wet fuels, the grate should have a length of 18–60 m instead of the actual 8 m).
- The temperature of the grate near the fuel inlet measured at the 31 MW furnace was too high for counter-current behaviour.
- Heavy evolution of "smoke" was visually observed near the fuel inlet at the 31 MW grate furnace.

In co-current combustion the primary air must first pass a char layer. Hence the burning behaviour of this layer is most important and will control the rest of the bed. It will therefore be analyzed in the following section.

2.1. *Combustion of char*

Cooper and Hallett [23] have simulated the combustion of char particles in an overfed fixed bed using a very detailed model and presented typical results for steady-state operation. Since the overfed fixed bed is comparable to the lowest layer of co-current combustion, the results are valid for it, too. Two results in particular are crucial:

- Char oxidation is a heterogeneous reaction and hence limited by temperature and diffusion. However, "it appears that as long as steady combustion is achieved char oxidation is substantially diffusion controlled, as assumed by many other investigators, and therefore largely independent of char reactivity" [23].
- The temperature near the bottom of the bed is nearly independent of the primary air mass flux. At first glance this is surprising, because more air certainly increases the combustion rate. But on the other hand the higher airflow

also increases the convective heat transport and this counteracts the first effect. Section 3.1 will make use of this fact.

Let us take a closer look at the first point. A typical model of char oxidation can be found in [9]

$$\frac{d\rho_c}{dt} = k_0 p_{O_2} \rho_c \tag{1}$$

with the density of char ρ_c, the partial pressure of oxygen p_{O_2} and the overall reaction rate constant k_0 (although it is actually not a constant):

$$k_0 = \frac{1}{\frac{1}{k_c} + \frac{RT\rho_c}{\Phi M_C A_p}\frac{1}{k_d}} \tag{2}$$

with the char reaction rate constant k_c, the ideal gas constant R, the temperature T, the stoichiometric ratio of char conversion

$$\Phi = \frac{1 + CO_2/CO}{0.5 + CO_2/CO} \tag{3}$$

(with the CO_2–CO concentration ratio CO_2/CO), the molecular weight of carbon M_C, the specific surface area of particles A_p and the mass transfer coefficient k_d. The char reaction rate constant k_c could be modelled using an Arrhenius-type relation

$$k_c = A_c \exp\left(-\frac{E_c}{RT}\right) \tag{4}$$

(with the pre-exponential factor A_c and the activation energy E_c), but as already stated, the overall reaction rate should only be diffusion limited ($k_c \to \infty$), so Eq. (1) becomes:

$$\frac{d\rho_c}{dt} = k_d \frac{\Phi M_C A_p}{RT} p_{O_2}. \tag{5}$$

The mass transfer coefficient k_d depends on various other values and will be further investigated in the next section.

2.1.1. *Mass transfer coefficient*

Many different possibilities of modelling the mass transfer coefficient can be found in the literature. One possibility is [9]

$$k_d = \frac{D^{2/3} u_g}{\nu^{2/3}\phi}\left(\frac{0.765}{Re^{0.82}} + \frac{0.365}{Re^{0.386}}\right) \tag{6}$$

with the superficial gas velocity u_g, the kinematic viscosity ν, the bed porosity ϕ, the Reynolds number

$$Re = \frac{u_g d_p}{\nu} \tag{7}$$

(with the particle diameter d_p) and the diffusion coefficient D:

$$D = 0.207 \times 10^{-4}\left(\frac{T}{300}\right)^{1.75}. \tag{8}$$

Another possibility is

$$k_d = \frac{D}{d_p}\left(2 + 1.1\, Sc^{1/3} Re^{0.6}\right) \tag{9}$$

with the Schmidt number

$$Sc = \frac{\nu}{D}, \tag{10}$$

although the value used in [8] is slightly corrected for the outflow of gases. A further possibility can be found in [24]

$$k_d = \frac{2.06 c_{pg} u_g}{\phi} Re^{-0.575} Sc^{-2/3} \tag{11}$$

with a dimensionless correction factor c_{pg}. A closer examination of the formulas reveals that, assuming a constant gas composition, the mass transfer coefficient only depends on the temperature and the gas flow. The mass transfer coefficient for air as a function of temperature T and primary air flow rate $\dot{m}_f$ using Eq. (6) is depicted in Fig. 2 (other values of φ, d_p, p_0 and the effective area for air flow per grate area certainly affect the absolute value of k_d, but the qualitative shape of the function remains nearly the same).

Although Eqs. (6), (9) and (11) look completely different, their resulting mass transfer coefficients are very similar – which is *not* surprising because all three ought to represent reality. And although all three equations are quite sophisticated, the much simpler equation

$$k_d = c_k T \dot{m}_f^{q_k} \tag{12}$$

(with appropriately chosen constant parameters c_k and q_k) characterizes the mass transfer coefficient remarkably well. Using this simplified relation in (5) provides the simple differential equation:

$$\frac{d\rho_c}{dt} = c_k \frac{\Phi M_C A_p}{R} \dot{m}_f^{q_k} p_{O_2}. \tag{13}$$

A constant stoichiometric ratio of char conversion Φ and constant bed porosity ϕ are common assumptions in the literature (e.g. [9]). The specific surface area of particles A_p is affected by particle shrinkage, but can be assumed to be constant, too, as the space left by diminishing particles is continuously filled with bigger particles (otherwise the assumption of constant bed porosity ϕ could not be held). Hence Eq. (13) implies the following surprising facts: the rate of char combustion

- Depends only on the primary air flow rate and the partial pressure of oxygen, but

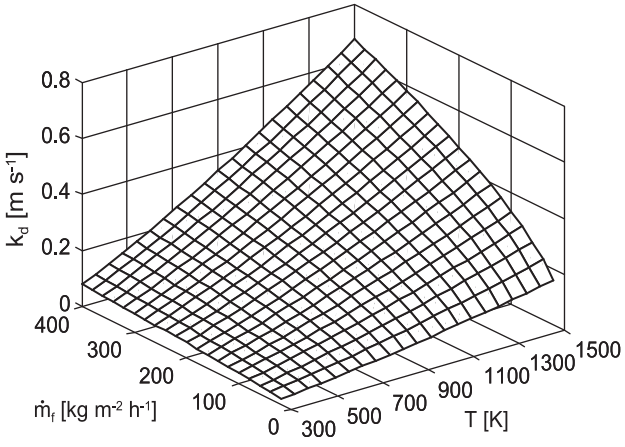

Fig. 2 – Mass transfer coefficient k_d as a function of temperature T and primary air flow rate $\dot{m}_f$ ($\phi = 0.5$, $d_p = 0.01$ m, $p_0 = 101{,}325$ Pa, effective area for air flow per grate area 0.1).

- Does *not* depend on temperature (using the common assumption of negligible pressure differences across the packed bed, e.g. [5,6,12,22,23]) and
- Does *not* depend on the density of char (as long as any is left).

Section 3.2 will make use of these facts.

3. Model

It is obvious that the dynamic behaviour is completely different for the counter-current and co-current case. Prior to modelling, it is therefore important to determine the present combustion situation at the pilot scale furnace investigated. As the experiments described later (Section 5.1) will prove, the plant studied definitely shows co-current behaviour with biofuel and operation conditions as specified in Section 4.

Based on the insight gained into the basic combustion situation, a simple model for co-current combustion (ignition at the bottom of the bed) will be derived in this section, in which results of both literature search and experiments are considered.

3.1. *Water evaporation*

In the co-current combustion situation, most of the water evaporates in a region marked ''water evaporation zone'' in Fig. 3.

The moist fuel entering the furnace is heated up due to heat conduction along the grate bars, but passes the ''dead'' zone nearly unchanged. The water evaporation zone begins roughly with the first emergence of dry fuel and ends with the disappearance of moist fuel, although the major part of water evaporation takes place in the first half of the zone (compare with simulation results in [22]). The energy for water evaporation is mainly provided by the combustion of a relatively thin layer of char near the surface of the grate. The major part of the energy must be conducted through the grate bars, hence water evaporation is limited by heat conduction in the grate. As already stated in Section 2.1, the temperature near the bottom of the char layer is almost independent of the primary air mass flux. Thus the rate of water evaporation is mainly independent of the primary air flow as well. This quite surprising finding will be verified by experiments (see Section 5.2).

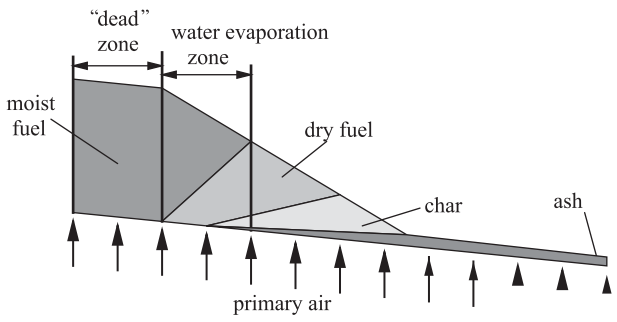

Fig. 3 – Water evaporation zone in co-current combustion.

The formulation of the model for water evaporation begins with a simple mass balance for the water m_w in the water evaporation zone

$$\frac{dm_w(t)}{dt} = -\dot{m}_{wev}(t) + \dot{m}_{w,in}(t) \tag{14}$$

with the water flow rate $\dot{m}_{w,in}$ entering the water evaporation zone and the water evaporation rate $\dot{m}_{wev}$ at time t, respectively. The water evaporation rate is assumed to be proportional to the current mass of water. This is a common approach in the literature, e.g. [8,25,26], and *not* a contradiction to the above mentioned energy limitation since the mass m_w of water influences the length of the dead zone (this will be discussed in the following) as well as the length and position of the water evaporation zone - bearing in mind that in steady state the complete energy for water evaporation must originate from the combustion process. As mentioned before, the rate of water evaporation is independent of the primary air flow, but experiments show that a certain dependence on the current position of the moving grate should be taken into account. This is done by a dimensionless scaling factor α_{wev}, which varies with the grate movement and averages 1. Together with the proportional constant c_{wev} one obtains:

$$\dot{m}_{wev}(t) = c_{wev} m_w(t) \alpha_{wev}(t). \tag{15}$$

In the next step the water flow rate $\dot{m}_{w,in}$ entering the water evaporation zone will be investigated, which will be the more challenging part. Let $\dot{m}_{w,inlet}(\tau)$ be the water of the moist fuel flow which enters the furnace at time τ. For mathematical convenience, it is meaningful to define the cumulating water mass

$$m_{w,inlet}(t) = \int_0^t \dot{m}_{w,inlet}(\tau) d\tau, \tag{16}$$

which is zero for a defined starting time and increases permanently. Before the water can cause a major effect, it must pass the dead zone, a process which takes some time. This dead time is denoted by T_d and will vary with time due to different conditions in the furnace. Hence by time t the cumulating water mass $m_{w,\ inlet}(t - T_d(t))$ has entered the water evaporation zone. The corresponding water flow rate $\dot{m}_{w,in}$ is obtained by differentiating:

$$\dot{m}_{w,in}(t) = \frac{dm_{w,inlet}(t - T_d(t))}{dt}. \tag{17}$$

Finally the dead time T_d must be characterized, which is done by means of two theoretical considerations, assuming a steady state condition with constant dry biofuel flow, constant moisture content and therefore a constant dead time.

- At first, the effect of increasing the moisture content is investigated, leaving the dry biomass flow unaltered. Initially, nothing will happen until the wetter fuel has passed the dead zone. Then the water evaporation zone becomes wetter and will shift away from the fuel inlet, because the heat conducted through the grate bars is already dissipated further downstream. Thus, more water in the water evaporation zone implies a longer dead time.

- In the second case the dry biofuel flow is increased, whereas the water flow is left unaltered (so the moisture content must decrease). In steady state, the water evaporation rate, the water in the water evaporation zone and the length of the dead zone will be the same. But due to the fact that the dry biomass flow is approximately proportional to the volumetric moist biomass flow, the water will pass the dead zone faster. So a higher rate of dry biofuel flow implies a shorter dead time.

In summary, a simple relation for the dead time (which will be verified by experiments in Section 5.2) would be

$$T_d(t) = c_d \frac{m_w(t)}{\dot{m}_{ds,inlet}(t)} \tag{18}$$

with the constant c_d.

3.2. Thermal decomposition of dry fuel

In co-current combustion, devolatilization and char burnout of the dry biomass take place in a region marked "thermal decomposition zone" in Fig. 4. It begins with devolatilization at the first emergence of dry fuel and ends with the complete burnout of char. The major part of devolatilization takes place in the region with overlapping dry fuel and char (compare with simulation results in [22]). As already assumed for water evaporation, a "dead" zone obviously also exists for the dry biomass.

In the case of the furnace studied, it turned out that it is sufficient to use only one zone for modelling thermal decomposition. In furnaces with air staging below the grate, it might be necessary to divide the grate into more zones for a better modelling of the dynamic response of thermal decomposition. In steady state, however, a model with only one zone is always guaranteed to be correct.

The formulation of the model for devolatilization and char burnout begins again with a simple mass balance, this time for the dry biomass m_{ds} (ash free) in the thermal decomposition zone

$$\frac{dm_{ds}(t)}{dt} = -\dot{m}_{thd}(t) + \dot{m}_{ds,in}(t) \tag{19}$$

with the thermal decomposition rate $\dot{m}_{thd}$ and the dry biomass flow rate $\dot{m}_{ds,in}$ entering the zone at time t, respectively. The biomass must pass the dead zone first, so it is reasonable to use the same approach as in Section 3.1:

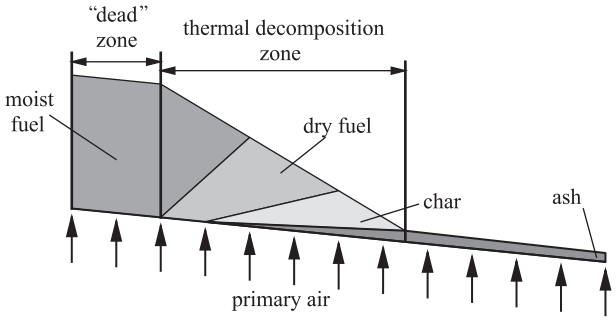

Fig. 4 – Thermal decomposition zone in co-current combustion.

$$\dot{m}_{ds,in}(t) = \frac{dm_{ds,inlet}(t - T_d(t))}{dt} \tag{20}$$

with the cumulating dry biomass

$$m_{ds,inlet}(t) = \int_0^t \dot{m}_{ds,inlet}(\tau)d\tau, \tag{21}$$

based on the dry biomass flow rate $\dot{m}_{ds,inlet}$ at the fuel inlet. The dead zone is the same as that for water evaporation (compare Figs. 3 and 4). Therefore, Eq. (18) is also advisable in this case, which is confirmed by experiments as well.

In the next step the thermal decomposition rate $\dot{m}_{thd}$ must be characterized. This is assumed to be proportional to the current mass of dry biomass m_{ds}, and experiments again show that a certain dependence on the current position of the moving grate should be taken into account. This is done by the dimensionless scaling factor α_{thd}, which averages 1. Furthermore, as the lower char layer produces the heat responsible for devolatilization, the primary air flow rate $\dot{m}_{pa}$ has a significant impact (see Section 2.1). This impact could be investigated by simulation using Eq. (13) as a basis for a detailed model of the thermal decomposition zone including the dry fuel above the char. This would be relatively complicated and error-prone due to potential improper simplifications. A more empirical approach is thus used here. A close examination of Eq. (13) reveals that the influence of the primary air flow rate is *multiplicative*. Hence it can be assumed that the overall effect of the primary air flow rate on the thermal decomposition rate can be specified with a curious, yet unknown function $f(\dot{m}_{pa})$ of the primary air flow rate being *multiplied* by the "rest":

$$\dot{m}_{thd}(t) = \underbrace{\tilde{c}_{thd} m_{ds}(t) \alpha_{thd}(t)}_{\text{"rest"}} \cdot f(\dot{m}_{pa}) \tag{22}$$

This function must be identified experimentally. For this reason, the air flow has been decreased and increased for such short periods of time (20 s) that the "rest" can be assumed to remain constant (see Section 4). These experiments were conducted several times at full (Fig. 11(e) and (f)) and partial load. The averaged thermal decomposition rate $\dot{m}_{thd}$ for different primary air flow rates $\dot{m}_{pa}$ is shown in Fig. 5. As the "rest" is an unknown constant (different for full and partial load), Fig. 5 strongly suggests the affine dependence

$$f(\dot{m}_{pa}) = c_f(\dot{m}_{pa} + \dot{m}_{pa,0}) \tag{23}$$

for a wide range of primary air flow rates including all typical operating conditions. With the abbreviation

$$c_{thd} := \tilde{c}_{thd} c_f \tag{24}$$

for the constants $\tilde{c}_{thd}$ and c_f the final equation for the thermal decomposition rate is obtained:

$$\dot{m}_{thd}(t) = c_{thd} m_{ds}(t) \alpha_{thd}(t) \left[\dot{m}_{pa}(t) + \dot{m}_{pa,0}\right]. \tag{25}$$

3.3. Resulting equations

In summary, the resulting mathematical model consists of only two ordinary differential equations, which represent the mass balances for the water in the water evaporation zone

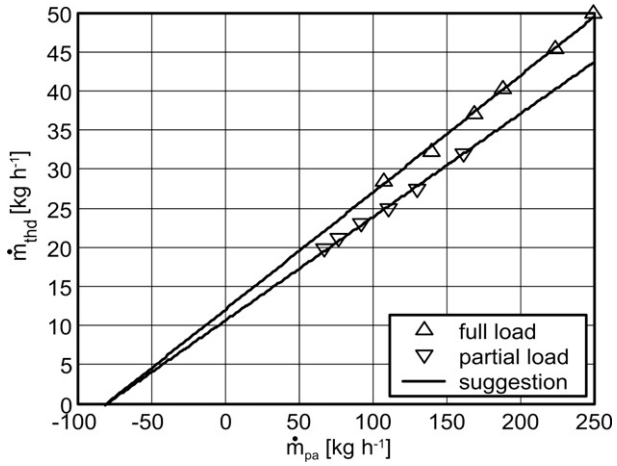

Fig. 5 – Averaged thermal decomposition rate $\dot{m}_{thd}$ for different primary air flow rates $\dot{m}_{pa}$ at full and partial load (negative values of $\dot{m}_{pa}$ are shown for mathematical convenience).

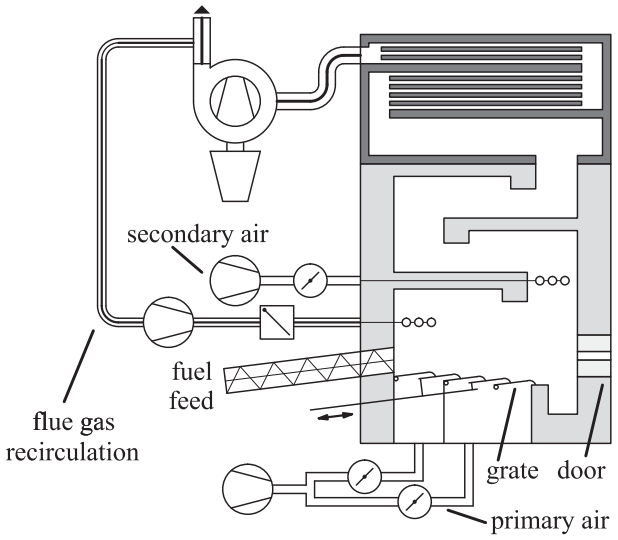

Fig. 6 – Furnace at the BIOENERGY 2020+.

and the dry biomass in the thermal decomposition zone respectively:

$$\frac{dm_w(t)}{dt} = -c_{wev} m_w(t) \alpha_{wev}(t) + \frac{dm_{w,inlet}(t - T_d(t))}{dt} \quad (26)$$

$$\frac{dm_{ds}(t)}{dt} = -c_{thd} m_{ds}(t) \alpha_{thd}(t) \left[\dot{m}_{pa}(t) + \dot{m}_{pa,0}\right] + \frac{dm_{ds,inlet}(t - T_d(t))}{dt} \quad (27)$$

with

$$T_d(t) = c_d \frac{m_w(t)}{\dot{m}_{ds,inlet}(t)}, \quad (28)$$

$$m_{w,inlet}(t) = \int_0^t \dot{m}_{w,inlet}(\tau) d\tau, \quad (29)$$

$$m_{ds,inlet}(t) = \int_0^t \dot{m}_{ds,inlet}(\tau) d\tau. \quad (30)$$

4. Experimental

All experiments were conducted at a pilot scale furnace (Fig. 6) of the research centre BIOENERGY 2020+. The pilot plant is a downscaled version (180 kW_{th}) of a typical medium scale furnace in terms of geometry and instrumentation. It is equipped with a screw conveyor, a horizontally moving grate (1 m long and 0.45 m wide), two primary air zones and a flue gas recirculation system above the grate.

The fixed bed can be visually observed through a view-glass in the furnace door at the opposite side of the fuel inlet (see Fig. 6). Furthermore, the bed can be partly removed through the furnace door with a shovel, so that a cross section (perpendicular to the centre-line of the grate) of the fixed bed can be visually observed.

The biofuel used was wood chips (mixture of oak, chestnut and pine) with an average moisture content of 21% (w.b.) and a typical composition for wood (carbon 49% (d.b.), hydrogen 6% (d.b.), oxygen 44% (d.b.) and ash 1% (d.b.)). Additionally, wet biomass (moisture content 61% (w.b.)) was prepared by soaking the wood chips in water for approximately 48 h. Dry biomass (zero moisture content) was prepared by drying at 378 K for 48 h.

The experiments were conducted under steady state conditions at full and partial load. At full load, experiments involved a moist biomass mass flow of 47 kgh^{-1} (equals 182 kW fuel heat emission), a primary air mass flow of 169 kgh^{-1} ($\lambda_{pa} = 0.79$) and a secondary air mass flow (including air leakage) of 187 kgh^{-1} ($\lambda = 1.66$). At partial load, the values were 29 kgh^{-1} (112 kW), 92 kgh^{-1} ($\lambda_{pa} = 0.69$) and 167 kgh^{-1} ($\lambda = 1.96$), respectively. Different air distributions between the two primary air zones were applied, but had no effect. This might be due to insufficient sealing between the zones.

Under these steady state conditions, the major input values (moisture content, biomass mass flow and primary air mass flow) were changed stepwise for short periods (20, 60 and 550 s) at full and partial load. To ensure stepwise changes of the moisture content, the automatic feeding system was partly disabled and the wet or dry biomass was fed manually into the screw conveyor. Biomass flow was varied (±30%) by modifying the rotational speed of the screw conveyor. Stepwise changes of the air flow (in the range of about ±10–±50%) were achieved by partly covering and uncovering the air inlet of the fan (compare with Section 5.2).

Primary and secondary air flows were measured by hot-film air mass sensors (Bosch HFM 2), the oxygen content of the flue gas was measured using a wide band lambda sensor (Bosch LSU 4.9), and a hygrothermal transducer (Jumo 907023/25) was used to determine the water vapour content of the flue gas. Precautions were taken to minimise air leakage, less than 2% and 12% was achieved at full and partial load, respectively. Furthermore, the current leakage air mass flow was determined with a model similar to those described in [27]. The fuel flow at the furnace inlet was not measured, but assumed to be proportional to the rotational speed of the screw conveyor. Additionally, the temperature of the grate at the fuel inlet was measured by a sensor placed on the bottom side of the grate. All values were recorded every second.

A combustion calculation was performed to obtain the current rate of water evaporation and the current rate of thermal decomposition of the biomass based on the current air mass flows, the current oxygen and water vapour content of the flue gas as well as the results of dry fuel analysis. Therefore, some assumptions had to be made: (i) complete combustion achieved by proper choice of combustion conditions; (ii) constant composition of the dry biofuel, which was shown to be valid by multiple biomass sampling for dry fuel analysis, and finally, (iii) simultaneous devolatilization and char burnout, which is ensured in steady state and approximately achieved otherwise, as the experiments were performed under steady state conditions.

5. Results

5.1. *Basic combustion behavior*

At first the fixed bed was visually observed through the viewglass in the furnace door at the opposite side of the fuel inlet during steady-state operation at full and half load as specified in Section 4. The picture was similar to [21]: no flames were visible in the first part of the bed, but a large amount of ''smoke'' rose from the bed (see Fig. 7).

However, the strains seem to consist of condensed water vapour (i.e. fog), because they disappear quickly above the bed. But how does this ''fog'' form? The primary air must be heated, saturated with water vapour and, most importantly, *cooled again*. In the counter-current case, the primary air is not heated until it reaches the vicinity of the reaction front, the essential cooling is missing completely. The situation is entirely different for the co-current case: the air is heated by the hot grate, enriched with water from the moist fuel and subsequently cooled down by the moist fuel (compare with Fig. 1). Furthermore the radiation from above the bed (which causes counter-current combustion in the first place) is absorbed by the ''fog'' close to the surface, which then disperses. Therefore, the radiation does not reach the surface of the bed and cannot ignite the bed at the top - hence no flames are visible in the first part of the bed.

Fig. 8 – Picture of the cross section of the bed 0.45 m (45% of grate length) downstream of the fuel inlet (a. char, b. dry fuel).

In the next step, the temperature of the grate at the fuel inlet was measured at full and half load and was found to be above 400 K – another indication for co-current combustion.

Finally the fixed bed was partly removed through the furnace door (as described in Section 4) during steady-state operation at full load and the cross section was visually inspected. It must be remarked that the removal process takes a few minutes, so the pictures do not show the accurate condition at normal operation but they do give very good clues of it. Figs. 8 and 9 show the cross sections of the bed at a distance of 0.45 m (45% of grate length) and 0.3 m (30% of grate length) from the fuel inlet, respectively. In both pictures the glowing char particles at the bottom of the bed can be seen clearly. Furthermore, the height of the char layer decreases with decreasing distance from the fuel inlet.

Fig. 7 – Picture of the fuel bed at full load through the viewglass at the opposite side of the fuel inlet (a. first part of the bed without flames but with water vapour fog).

Fig. 9 – Picture of the cross section of the bed 0.3 m (30% of grate length) downstream of the fuel inlet (a. char, b. dry fuel).

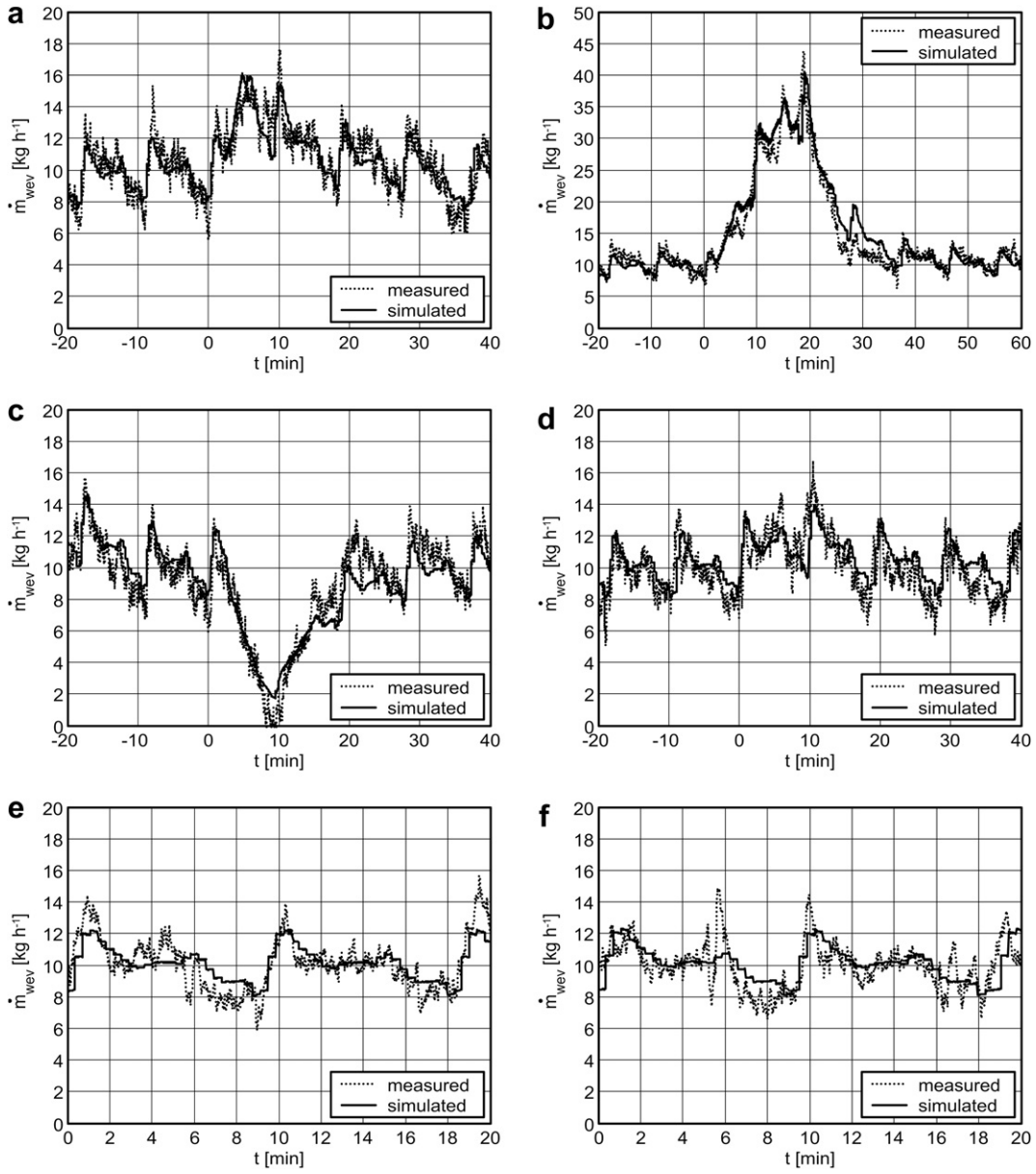

Fig. 10 – Comparison of measured and simulated water evaporation rate: (a) short increase of moisture content (at $t = 0$ the moisture content w is increased from 21 to 61% for 60 s while leaving $\dot{m}_{ds,inlet}$ unaltered); (b) long increase of moisture content (at $t = 0$ the moisture content w is increased from 21 to 61% for 550 s while leaving $\dot{m}_{ds,inlet}$ unaltered); (c) long decrease of moisture content (at $t = 0$ the moisture content w is decreased from 21 to 0% for 550 s while leaving $\dot{m}_{ds,inlet}$ unaltered); (d) increase of moist biofuel flow (at $t = 0$ the moist biofuel mass flow is increased from 47 to 61 kgh^{-1} for 550 s while leaving w unaltered); (e) decrease of air flow (at $t = 5$ and 16 min the air flow $\dot{m}_{pa}$ is decreased from 169 to 107 kgh^{-1} for 20 s); (f) increase of air flow (at $t = 5$ and 16 min the air flow $\dot{m}_{pa}$ is increased from 169 to 250 kgh^{-1} for 20 s).

The plant studied thus definitely shows co-current behaviour with biofuel and operating conditions as specified in Section 4.

5.2. *Model verification*

Experiments were conducted as specified in Section 4 in order to identify the coefficients (c_{wev}, α_{wev}, c_d, c_{thd}, α_{thd} and $\dot{m}_{pa,0}$) and to validate the model. Based on a steady state condition, the major input values (moisture content, biomass mass flow and primary air mass flow) were changed stepwise for short periods at full and partial load. The coefficients of the model were determined using a numerical optimization algorithm with quadratic cost function.

The results for the water evaporation and thermal decomposition rates at full load ($\dot{m}_{pa} = 169$ kgh^{-1} and moist biomass mass flow of 47 kgh^{-1} – hence $\dot{m}_{w,inlet} = 10$ kgh^{-1} and $\dot{m}_{ds,inlet} = 37$ kgh^{-1} $= 37$ kgh^{-1} as $w = 21\%$) are shown in Figs. 10 and 11, respectively (the charts at the same position (e.g. Figs. 10(a) and 11(a)) always belong to the same experiment). The first three charts – (a), (b) and (c) – show the rates for variations in moisture content, charts (d) show the rates for

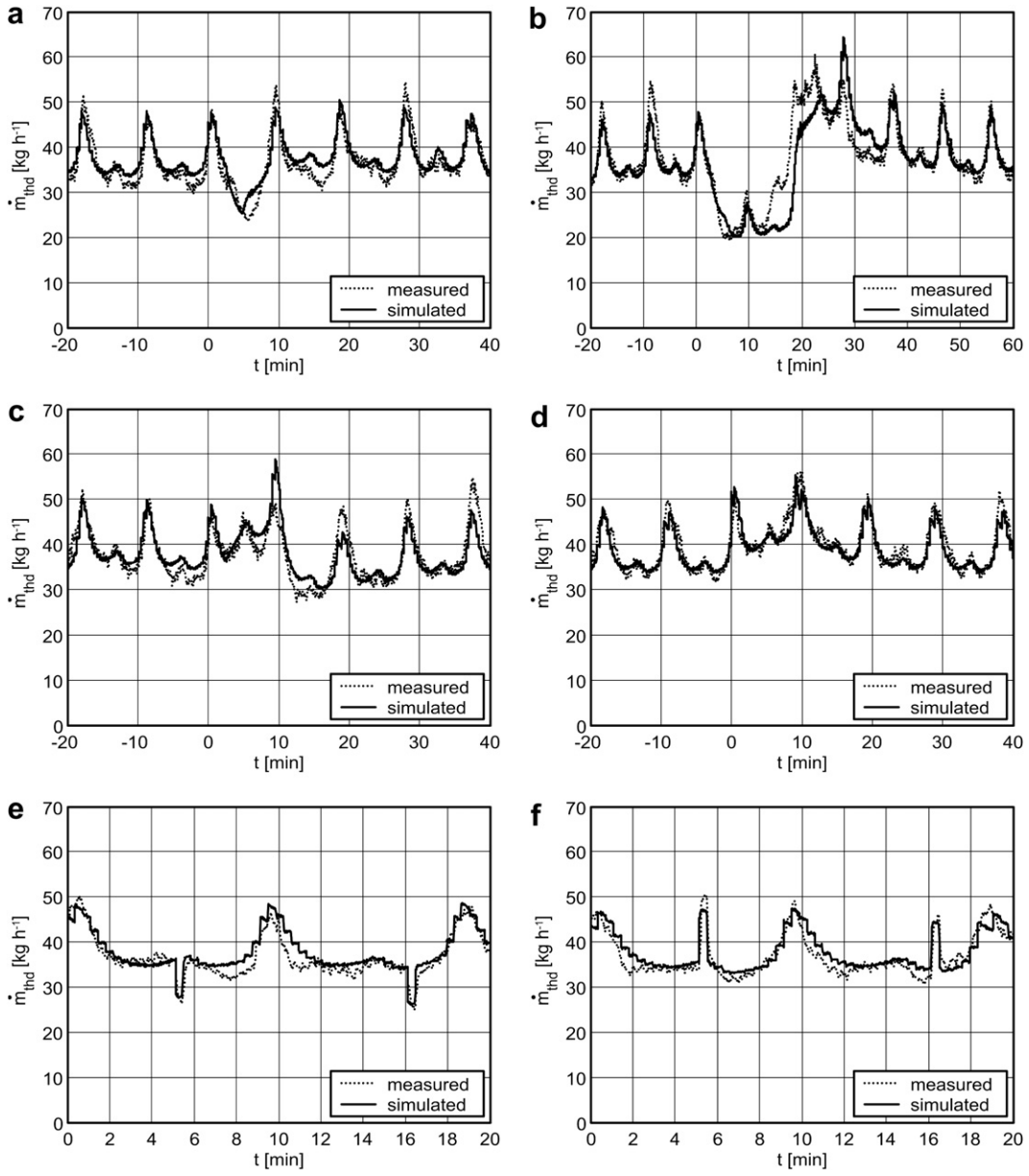

Fig. 11 – Comparison of measured and simulated thermal decomposition rate: (a) short increase of moisture content (at $t = 0$ the moisture content w is increased from 21 to 61% for 60 s while leaving $\dot{m}_{ds,inlet}$ unaltered); (b) long increase of moisture content (at $t = 0$ the moisture content w is increased from 21 to 61% for 550 s while leaving $\dot{m}_{ds,inlet}$ unaltered); (c) long decrease of moisture content (at $t = 0$ the moisture content w is decreased from 21 to 0% for 550 s while leaving $\dot{m}_{ds,inlet}$ unaltered); (d) increase of moist biofuel flow (at $t = 0$ the moist biofuel mass flow is increased from 47 to 61 kgh^{-1} for 550 s while leaving w unaltered); (e) decrease of air flow (at $t = 5$ and 16 min the air flow $\dot{m}_{pa}$ is decreased from 169 to 107 kgh^{-1} for 20 s); (f) increase of air flow (at $t = 5$ and 16 min the air flow $\dot{m}_{pa}$ is increased from 169 to 250 kgh^{-1} for 20 s).

increased moist biofuel mass flows and the last two charts – (e) and (f) – show the rates for variations in air flow.

The measured and simulated rates match very well, even though some variations (especially the long variations in moisture content – (b) and (c)) are really challenging and far beyond normal operating conditions.

The suggested relation for the dead time (Eq. (18)) works properly, as can be seen particularly in Fig. 10(a)–(c).

As already mentioned (Sections 3.1 and 3.2), primary air flow has almost no effect on the water evaporation rate (Fig. 10(e) and (f)), but a crucial impact on the thermal decomposition rate (Fig. 11(e) and (f)).

For partial load the measured and simulated rates match as well as in the full load case, hence they can be omitted.

6. Discussion

It has been shown that the combustion of wood chips on a horizontally moving grate exhibits co-current combustion

behaviour as depicted in Fig. 12. The radiation from flames and furnace walls cannot reach the surface of the first part of the fuel bed as it is absorbed by a layer of fog resulting from co-current combustion. Very dry fuel results in less fog, so a reaction front moving downwards might evolve additionally, but will be much slower than the reaction area moving upward (see Fig. 1). The combustion behaviour might be different for other biofuels than wood chips.

Subsequently, a simple but quite accurate model for co-current grate combustion was derived from physical considerations. Although the main focus is an accurate description of the dynamic behaviour (i.e. response to changes of input values), the model is guaranteed to be correct in steady state as it is based on mass balances (in steady state, the same amount of mass enters and leaves the furnace).

Devolatilization and char burnout were modelled with only one zone, which turned out to be sufficient for the pilot scale plant. In the furnaces with air staging below the grate it might be necessary to use more zones for a better modelling of the dynamic response. In steady state, however, a model with only one zone is always guaranteed to be correct.

The model consists of only two ordinary differential equations specifying the rate of water evaporation and the rate of thermal decomposition of dry biomass, hence it is particularly suitable as a basis for model based control strategies. It is the core piece of an overall model and intended to be used together with other sub-models: a model characterizing the correlation of pressure drop and volumetric flow rate [27], a model describing the relation between actual temperatures and values measured by temperature sensors [28] and a model for gas tube heat exchangers [29]. Finally the resulting overall model can be used as a basis for the design of a model based control strategy, such as differential geometric techniques or Lyapunov-based approaches [1–4].

The model was validated by comparison of measured and simulated values at a pilot scale plant (180 kW_{th}). Since the investigated plant is a downscaled version of a typical medium scale furnace in terms of geometry and instrumentation, the model is also applicable to medium scale furnaces.

Flue gas recirculation below the grate was not investigated and hence is not included in the model. It is supposed that this can be done by modifying the multiplicative function of the thermal decomposition rate (Eq. (23)) since recirculated flue gas basically increases the gas mass flux and decreases the partial pressure of oxygen (see Eq. (13)). However this should be verified by experiments.

Preheated combustion air was also not investigated and is not included in the model. It is supposed that preheated combustion air mainly influences the water evaporation rate $\dot{m}_{wev}$ in Eq. (15) and thus the mass of water in the water evaporation zone as well as the length of the dead zone, but this should also be verified experimentally.

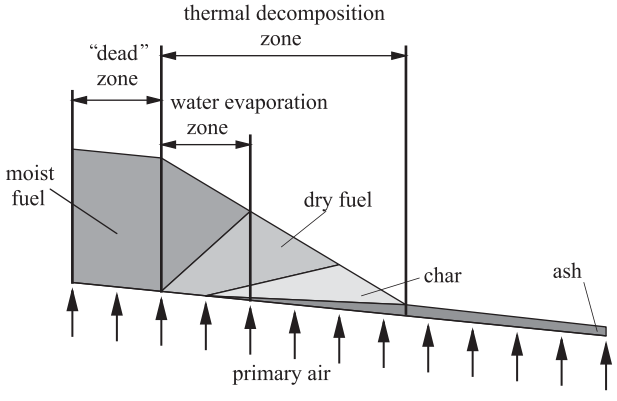

Fig. 12 – Co-current combustion behaviour with dead zone, water evaporation zone and thermal decomposition zone.

7. Conclusions

The considerations and results presented strongly suggest the hypothesis that the combustion of wood chips in grate furnaces shows co-current behaviour with ignition at the bottom of the bed. The main criteria are high grate temperatures ($T > 373$ K) at the fuel inlet as well as water vapour fog and the absence of flames in the first part of the fuel bed.

The work performed for the first time provides a mathematical model of grate combustion based on physical considerations, which is suitable as a basis for model based control strategies. Model based control strategies are by far the most sophisticated approach to biomass furnace control. Therefore their future implementation would lead to a significant improvement in the operating performance of biomass furnaces.

To increase the range of application of the model it will be necessary to investigate the influence of flue gas recirculation below the grate, preheated combustion air and air staging below the grate. The work already performed provides a comprehensive basis for these investigations.

Acknowledgements

This article is the result of a project carried out in cooperation with BIOENERGY 2020+ (a research centre within the framework of the Austrian COMET programme), which is funded by the Republic of Austria as well as the federal provinces of Styria, Lower Austria and Burgenland.

Nomenclature

A_c	pre-exponential factor [$Pa^{-1}\,s^{-1}$]
A_p	specific surface area of particles [$m^2\,m^{-3}$]
c	rate constant [s^{-1}]
c_d	dead time constant [–]
D	diffusion coefficient [$m^2\,s^{-1}$]
d_p	particle diameter [m]
E_c	activation energy [$J\,mol^{-1}$]
k_0	overall reaction rate constant [$Pa^{-1}\,s^{-1}$]
k_c	char reaction rate constant [$Pa^{-1}\,s^{-1}$]
k_d	mass transfer coefficient [$m\,s^{-1}$]
M_C	molecular weight of carbon [$kg\,mol^{-1}$]
m	mass [kg]
$\dot{m}$	mass flow rate [$kg\,s^{-1}$]

$\dot{m}_f$	primary air flow rate [kg m^{-2} s^{-1}]
p_0	ambient pressure [Pa]
p_{O_2}	partial pressure of oxygen [Pa]
R	ideal gas constant [J mol^{-1} K^{-1}]
Re	Reynolds number [–]
Sc	Schmidt number [–]
T	temperature [K]
T_d	dead time [s]
t	time [s]
u_g	superficial gas velocity [m s^{-1}]
w	moisture content (w.b.) [%]

Greek symbols

α	grate – dependent factor [–]
λ	air/fuel ratio [–]
ν	kinematic viscosity [m^2 s^{-1}]
ρ_c	density of char [kg m^{-3}]
τ	time [s]
Φ	stoichiometric ratio [–]
φ	bed porosity [–]

Abbreviations

d.b.	dry basis
w.b.	wet basis

Subscripts

ds	dry substance
in	at the beginning of a zone
inlet	at the fuel inlet
pa	primary air
sa	secondary air
thd	thermal decomposition
w	water
wev	water evaporation

REFERENCES

[1] Isidori A. Nonlinear control systems. Springer-Verlag; 1995.
[2] Bauer R, Dourdoumas N. Time-discrete approximative state linearization. Automatisierungstechnik 2007;55:1–9 [in German].
[3] Khalil H. Nonlinear systems. Prentice Hall; 2002.
[4] Slotine J, Li W. Applied nonlinear control. Prentice Hall; 1991.
[5] Fatehi M, Kaviany M. Adiabatic reverse combustion in a packed bed. Combustion and Flame 1994;99:1–17.
[6] Fatehi M, Kaviany M. Role of gas-phase reaction and gas-solid thermal nonequilibrium in reverse combustion. International Journal of Heat and Mass Transfer 1997;40: 2607–20.
[7] Gort R, Brouwers J. Theoretical analysis of the propagation of a reaction front in a packed bed. Combustion and Flame 2001;124:1–13.
[8] Johansson R, Thunman H, Leckner B. Influence of intraparticle gradients in modeling of fixed bed combustion. Combustion and Flame 2007;149:49–62.
[9] Lans R, Pedersen L, Jensen A, Glarborg P, Dam-Johansen K. Modelling and experiments of straw combustion in a grate furnace. Biomass and Bioenergy 2000;19:199–208.
[10] Saastamoinen J, Taipale R, Horttanainen M, Sarkomaa P. Propagation of the ignition front in beds of wood particles. Combustion and Flame 2000;123:214–26.
[11] Shin D, Choi S. The combustion of simulated waste particles in a fixed bed. Combustion and Flame 2000;121:167–80.
[12] Thunman H, Leckner B. Influence of size and density of fuel on combustion in a packed bed. Proceedings of the Combustion Institute 2005;30:2939–46.
[13] Wurzenberger J. A combined packed bed and single particle model applied to biomass combustion. Graz University of Technology; 2001.
[14] Yang Y, Goh Y, Zakaria R, Nasserzadeh V, Swithenbank J. Mathematical modelling of MSW incineration on a travelling bed. Waste Management 2002;22:369–80.
[15] Yang Y, Yamauchi H, Nasserzadeh V, Swithenbank J. Effects of fuel devolatilisation on the combustion of wood chips and incineration of simulated municipal solid wastes in a packed bed. Fuel 2003;82:2205–21.
[16] Yang Y, Ryu C, Khor A, Sharifi V, Swithenbank J. Fuel size effect on pinewood combustion in a packed bed. Fuel 2005; 84:2026–38.
[17] Yang Y, Ryu C, Khor A, Yates N, Sharifi V, Swithenbank J. Effect of fuel properties on biomass combustion – part II. Modelling approach – identification of the controlling factors. Fuel 2005;84:2116–30.
[18] Yang Y, Sharifi V, Swithenbank J. Converting moving-grate incineration from combustion to gasification – numerical simulation of the burning characteristics. Waste Management 2007;27:645–55.
[19] Zhou H, Jensen A, Glarborg P, Jensen P, Kavaliauskas A. Numerical modeling of straw combustion in a fixed bed. Fuel 2005;84:389–403.
[20] Van Kessel L. Stochastic disturbances and dynamics of thermal processes. Eindhoven Technical University; 2003.
[21] Thunman H, Leckner B. Ignition and propagation of a reaction front in cross-current bed combustion of wet biofuels. Fuel 2001;80:473–81.
[22] Thunman H, Leckner B. Co-current and counter-current fixed bed combustion of biofuel – a comparision. Fuel 2003; 82:275–83.
[23] Cooper J, Hallett W. A numerical model for packed-bed combustion of char particles. Chemical Engineering Science 2000;55:4451–60.
[24] Di Blasi C. Dynamic behaviour of stratified downdraft gasifiers. Chemical Engineering Science 2000;55:2931–44.
[25] Bryden K, Ragland K, Rutland C. Modeling thermally thick pyrolysis of wood. Biomass and Bioenergy 2002;22:41–53.
[26] Di Blasi C, Brance C, Sparano S, Mantia B. Drying characteristics of wood cylinders for conditions pertinent to fixed-bed countercurrent gasification. Biomass and Bioenergy 2003;25:45–58.
[27] Bauer R, Gölles M, Brunner T, Dourdoumas N, Obernberger I. Modelling of pressures and volume flows for a biomass furnace. Automatisierungstechnik 2007;55:404–10 [in German].
[28] Bauer R, Gölles M, Brunner T, Dourdoumas N, Obernberger I. What is really measured by temperature sensors in a biomass furnace? Automatisierungstechnik 2007;55:600–7 [in German].
[29] Bauer R, Gölles M, Brunner T, Dourdoumas N, Obernberger I. Dynamic modelling of the heat transfer in a gas tube heat exchanger. Automatisierungstechnik 2008;56:513–20 [in German].